Article

A general sensitive detecting strategy of ions through plasmonic resonance energy transfer from gold nanoparticles to rhodamine spirolactam

Ming Xuan Gao, Hong Yan Zou, Yuan Fang Li, and Cheng Zhi Huang

Anal. Chem., **Just Accepted Manuscript** • DOI: 10.1021/acs.analchem.6b04124 • Publication Date (Web): 10 Jan 2017

A general sensitive detecting strategy of ions through plasmonic resonance energy transfer from gold nanoparticles to rhodamine spirolactam

Ming Xuan Gao, [†] Hong Yan Zou, [‡] Yuan Fang Li, [†] Cheng Zhi Huang *, [†, ‡]

[†]Key Laboratory of Luminescent and Real-Time Analytical Chemistry, Ministry of Education, College of Chemistry and Chemical Engineering, Southwest University, Chongqing 400715, China.

[‡] College of Pharmaceutical Sciences, Southwest University, Chongqing 400715, China.

KEYWORDS plasmonic resonant energy transfer, localized surface plasmonic resonant scattering light, rhodamine spirolactam, gold nanoparticle, finite-difference time-domain

ABSTRACT: Plasmonic resonant energy transfer (PRET), which occurs between the plasmonic nanoparticles and organic dyes, has significant potential in target sensing chemistry owing to its sensitivity at single nanoparticle level. In this contribution, by using AuNPs, which has localized surface plasmonic resonance light scattering (LSPR-LS) around 550 nm, as the donor of PRET, a general sensitive detecting strategy of ions were developed. Targets can specifically react with a ring-close structured rhodamine spirolactam, which was prepared from rhodamines in the presence of different primary amine wherein the option of the primary amine is up to the targets, forming ring-open structured rhodamine spirolactam with the strong absorption around 550 nm. This process triggered the PRET from gold nanoparticles (AuNPs) to the ring-open structured rhodamine spirolactam. As a proof of concept, Cu^{2+} and Hg^{2+}were detected by using rhodamine B hydrazide and *N*-(rhodamine B)lactam-ethylenediamine, respectively. With the aids of dark field microscope, the LSPR-LS of AuNPs gets decreased within 10 min with the addition of Cu^{2+} or Hg^{2+}. The scattering light spectra get red shifted during the targets addition due to the quenching dip phenomenon. Further theoretical simulation indicated the PRET process could be aroused by the electric field diminishment of AuNPs via the interaction of rhodamine. This single nanoparticle based detecting strategy could be further applied for other anions, cations or small organic molecules detection by simply changing the rhodamine spirolactam.

As an early developed optical technique, resonance energy transfer (RET) has become a common tool for bio-analysis and bioimaging.[1-8] In RETs, two different chromophores acting as energy donor and acceptor respectively are interacting in the dipole-dipole manner and transferring the energy in a non-radiative behavior.[9,10] As a special instance, gold nanoparticles (AuNPs) are involved in the RET process acting as both donor and acceptor since their stability, accessibility and the unique localized surface resonant plasmon (LSPR) property.[11,12] When acting as an energy acceptor, the localized free electrons which generated the LSPR make the AuNPs interacting with other chromophores in a metal-dipole manner, and the energy can be transferred more efficient through a relative longer distance, such as the nanometal surface energy transfer.[10,13,14] The most interesting is that AuNPs can also act as an energy donor in the recent established plasmon resonance energy transfer (PRET) in 2007.[5]

For the occurrence of PRET, localized surface plasmonic resonance light scattering (LSPR-LS) of AuNPs is the essential prerequisite.[15] By using the LSPR-LS as the optical probe, single nanoparticle based sensing platform with high sensitivity and spatial resolution could be achieved.[16] Moreover, when highly spectra-overlapped chromophores were used as energy acceptor, the LSPR-LS of AuNPs can be quenched in a non-radiative manner and manifest as the diminishment of scattering light intensity, which is the PRET process.[17,18] This method is elegant and easy to be observed with a simple dark field microscope (DFM),[19,20] and it is widely applied for heavy metal detection,[21]cellular reactions,[22] and energy exchanges.[23] In the RET process, the highly luminescent ability of donor and the strong electronic transitions of both donor and acceptor are essential to its observation.[24] Benefiting from the LSPR property, the AuNPs has a much larger scattering crosssection than its physical crosssection, which is known as "plasmon-induced light

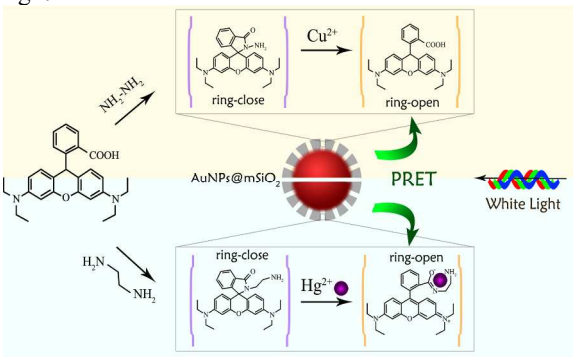

Scheme 1. Illustration of PRET based target detecting strategy between rhodamine spirolactam and AuNPs.

concentration" (PILC) effect.[25,26] It allows the AuNPs emit more energy and presents higher luminescence than fluorescent molecules.[27] However, suffering from the lack of appropriate energy acceptor chromophores, the construction of donor-acceptor (D-A) pair handicaps the development of this new founded RETs. In the previous reports, cytochrome *c* was commonly involved in this process to form the D-A pair.[17,28] However, for the development of PRET in analytical chemistry, cytochrome *c* could not satisfy the requirement of analytes identification or detection since few targets could cause the signal changes between this D-A pair. Therefore, it is worth to pursuit more of chromophores to form the D-A pairs.

Rhodamine and its derivatives, a common used fluorescent organic molecules (FOMs), attracted considerable interest from chemists and are widely applied in the biosensing and bioimaging.[29-33] Comparing to the traditional FOMs, rhodamine emerged a very unique property.[34] By forming the spirolactam structure, no apparent absorption band in the visible light range could be observed; however, when specific target existed, the spirolactam could be opened and exhibited strong absorption around 550 nm with the molar extinction coefficient over 8×10^4 $M^{-1} \cdot cm^{-1}$,[35] which overlapped with that of the LSPR-LS of AuNPs with 50 nm diameter (Scheme 1).[36] Long and his co-workers have pioneered the feasibility to generate PRET by using rhodamine and AuNPs.[37,38] Considering different optical probes which respond to different targets could be synthesized from different rhodamine spirolactam, series PRET-based sensing methods could be established between the rhodamine spirolactam derivatives and AuNPs. In this work, whereas the mercury ions are related to the pathogenic process of Minamata disease,[39,40]and copper ions are related to the Alzheimer's disease and Parkinson's disease,[41] we chose these two heavy metal ions to prove the concept of this general detecting method.

EXPERIMENTAL SECTION

Reagents. Chloroauric acid tetrahyrate ($HAuCl_4 \cdot 4H_2O$) was purchased from Sinopharm Chemical Reagent Co. Ltd. (Shanghai, China). Polyvinylpyrrolidone (PVP, MW ≈ 55,000), rhodamine B and tetraethyl orthosilicate (TEOS) were purchased from Sigma-Aldrich Co. LLC. (USA). All chemicals were of analytical reagent grade and used as received unless otherwise statements. Ultrapure water (18.2 MΩ·cm) which prepared with a Milli-Q system (Millipore, Bedford, USA) was used throughout the experiments.

Characterization. Scanning electron microscopy (SEM) images were recorded with S-4800 Scanning electron microscopy (Hitachi, Japan). Absorption and PL spectra were measured at room temperature with a 3600 UV-Vis-NIR spectrophotometer (Shimadzu, Japan) and a 2500 fluorescence spectrophotometer (Hitachi, Japan), respectively. ^1H and ^{13}C NMR spectra were recorded with AV-300 spectrometer (Bruker, German). Dark-field light scattering images were obtained through BX51 optical microscope (Olympus, Japan) equipped with dark-field condenser (U-DCW, 1.2-1.4) and DP72 single chip true-color CCD camera (Olympus, Japan), which was controlled by IPE software (MediaCybernetics, USA). The scattering lights from AuNPs were collected by a 100× object lens (adjustable numerical aperture from 0.6 to 1.3) and photographed by a 2070 × 1548 pixel true-color digital CCD camera. The acquired images were all 24-bit TIFF picture files.

Synthesis of gold nanoparticles. Gold nanoparticles (AuNPs) were synthesized according to a traditional method by reducing $HAuCl_4$ with sodium citrate. Briefly, 0.5 mL of 1 % (w/w) $HAuCl_4$ solution was added into 50 mL H_2O and brought to boiling. Then, 0.2 mL of 2 % (w/w) citrate sodium was added under vigorous stirring. The solution turned to violetred within 15 min. The mixture was kept boiling and refluxed for 5 minutes, then cool down to room temperature under continuous stirring. The solution was kept in 4 ^oC for further use.

Synthesis of mesoporous silica coated AuNPs (AuNPs@mSiO$_2$). To a 10 mL round flask, 1 mL as-synthesized 50 nm AuNPs and 4 mL H_2O were added and stirred. Then the aqueous solution was treated with 30 μL 27.8 mg/mL PVP and kept stirring for 24 h. The obtained conjugates were centrifuged at 8,000 rpm for 15 min once to remove excess PVP and the precipitates were resuspended in 5 mL ethanol for further use. To a 100 mL round flask, 40 mL ethanol, 10 mL H_2O and 5mL as-prepared PVP coated AuNPs were added and stirred in room temperature, then added 500 μL $NH_3 \cdot H_2O$ and 80 μL 10%(*v/v*) TEOS. Keeping the hydrolysis reaction for 6 h and added 500 μL $NH_3 \cdot H_2O$ and 150 μL 10%(*v/v*) TEOS, the mixture was kept stirring for another 6 h. The obtained silica coated AuNPs (AuNPs@SiO_2) were centrifuged at 8,000 rpm for 15 min. The as-prepared AuNPs@SiO_2 was redispersed in 20 mL H_2O and 1 mL 1g/mL NaOH aqueous solution was added to etching the silica shell for 16 h. The solution was centrifuged at 8,000 rpm for 15 min to ensure NaOH was removed completely. The final product was resuspended in 10 mL ethanol.

Synthesis of *N*-(rhodamine B)lactam-ethylenediamine (RhB-EDA). Rhodamine B (1g, 2 mmol) was dissolved in 20 mL methanol. Then ethylenediamine (1.8 mL, 2.7 mmol) was added in the solution dropwise. The mixture was stirred at reflux for 24 h until it turned orange and clear. The methanol was vacuum evaporated and left an orange viscous liquid. The crude product was dissolved in 100 mL 1 M HCl to generate a clear red solution and about 120 mL 1M NaOH was added into this aqueous solution slowly, with hand stirring until the solution reached pH 8−9, and a pink precipitate was formed. Then the final product was obtained by vacuum filtration and freeze drying (1.02 g, yield: 93%). ^1H NMR ($CDCl_3$, 400 MHz) δ (ppm): 7.90 (s, 1H), 7.45 (s, 2H), 7.09 (s, 1H), 6.44 (m, 6H), 3.34 (d, 8H, J = 20 Hz), 3.19 (s, 2H), 2.41 (s, 2H), 1.58 (b, 2H), 1.18 (t, 12H, J = 12 Hz); ^{13}C NMR ($CDCl_3$, 100 MHz) δ (ppm): 168.67, 153.49, 153.31, 148.86, 132.41, 131.25, 128.69, 128.06, 123.84, 122.78, 108.19, 105.70, 97.77, 64.98, 44.36, 43.84, 40.81, 12.60.

Synthesis of rhodamine B hydrazide (RhB-HA). The synthesis of rhodamine B hydrazide was based on the previous reports and modified slightly. Briefly, to 100 mL round flask 1.2 g (2.5mmol) rhodamine B, 3.0 mL 85 % (*v/v*) hydrazine hydrate and 30mL ethanol were added and stirred vigorously. The mixture was heated at 80 ^oC and refluxed for 2 h until the solution became clear light orange color, then cooled it down to room temperature. Solvent was removed by vacuum-rotary evaporation, and the crude product was dissolved in 50 mL 1 M HCl to get a clear red solution. Around 70 mL 1 M NaOH was slowly added to adjust the pH of this solution to 8-9 and the pink product precipitated. By washing and suction filtrating for three times, the final product could be obtained after the lyophilization (1.12 g, yield: 91 %). ^1H NMR ($CDCl_3$, 400 MHz) δ (ppm): 7.94 (m, 1H), 7.45 (m, 2H), 7.11 (m, 1H), 6.47 (m, 6H), 3.61 (b, 2H), 3.36 (q, 8H, J = 20 Hz), 1.18 (t, 12H, J = 16 Hz). ^{13}C NMR ($CDCl_3$, 100 MHz) δ (ppm): 166.15, 153.85, 151.55, 148.91, 132.51, 130.05, 128.10, 123.83, 122.99, 108.09, 104.64, 98.03, 65.90, 44.38, 12.60.

Loading rhodamine spirolactam derivatives to AuNPs@mSiO$_2$. To 1 mL AuNPs@mSiO$_2$ aqueous solution, 5×10^{-5}M (final concentration) rhodamine spirolactam derivatives ethanol solution was added and diluted with ethanol to 5 mL. Then, the mixture was kept shaking for 24 h (120 rpm, 25 ^{o}C). The obtained rhodamine doped AuNPs@mSiO$_2$ were centrifuged at 8,000 rpm for 15 min once to remove excess rhodamine spirolactam derivatives and the precipitates were resuspended in water for further use.

Observation of PRET in the rhodamine doped AuNPs@mSiO$_2$. Slide glass was pretreated with chromic acid, then rhodamine doped AuNPs@mSiO$_2$ was deposited on the surface of the slide glass. The as-prepared glass was put on the automatic stage and target-contained solution was added for observation.

Computational details. The FDTD simulations were performed on FDTD solutions 8.11.422 by Lumerical Solutions, Inc. According to the SEM images, the thickness of the shell was set to 10 nm. Total-field scattered-field source with 300-800 nm wavelength and perfectly matched layer were applied to this simulation. ε_{bg} was set at 1.7780 based on the use of water as a medium in the experiments.

RESULTS AND DISCUSSION

Synthesis and characterization of AuNPs@SiO$_2$ and AuNPs@mSiO$_2$. The purpose to generate mesoporous silica coated AuNPs (AuNPs@mSiO$_2$) was to load more rhodamine spirolactam derivatives due to the large specific surface area. Previous report has demonstrated that with assistance of PVP, smooth and homogeneous silica shell could be generated.[42] Therefore, PVP (MW ≈ 55,000) was adsorbed on the surface of AuNPs in advance and TEOS was hydrolysis in a Stöber-like growth process (Figure 1). Scanning electronic microscope (SEM) characterized the thickness of the silica shell was about 10 nm and the absorption spectra was also in accord with the SEM result by manifesting as a 14 nm bathochromic shift. This was because the coated silica shell altered the dielectric constant surrounding the AuNPs. Dynamic light scattering (DLS) measurement also presented an increase of the diameter (from 58.77nm to 122.41 nm) after the coating process. Previous work by other group has demonstrated the etching process of NaOH could generate mesoporous silica.[43] Therefore, same strategy was used here to further form mesoporous silica shell. Absorption spectrum manifested an 8 nm blue shift after the etching process comparing to the AuNPs@SiO$_2$. Also SEM and DLS were used to characterize the formation of AuNPs@mSiO$_2$. The thickness of mesoporous silica was about 8 nm and the contrast was relatively lower than the silica shell in SEM. The diameter in DLS shrunk to 91.28 nm due to the volume decrease in the etching process. All these evidences have clearly proved the success in the synthesis of AuNPs@mSiO$_2$.

Selectivity of rhodamine spirolactam derivatives. Since the specific coordination effect between the electrons of heteroatoms to targets, rhodamine spirolactam derivatives became the chemodosimeter in metal ions detection.[44-46] And the selectivity of rhodamine spirolactam derivatives was essential to that of the PRET-based detecting method. Therefore, as the keystone for target detection, the selectivity of those two as-synthesized rhodamine spirolactam molecules (RhB-HA and RhB-EDA) was firstly confirmed. Target ions (Cu^{2+} for RhB-HA, Hg^{2+} for RhB-EDA) were added to rhodamine spirolactam aqueous solutions (Figure S3). The spectra indicated the strong absorption band was aroused around 550 nm while the color of solutions turned to pink. However, 10 times excess interfering ions could not lead to significant spectral or optical signal changes. The results

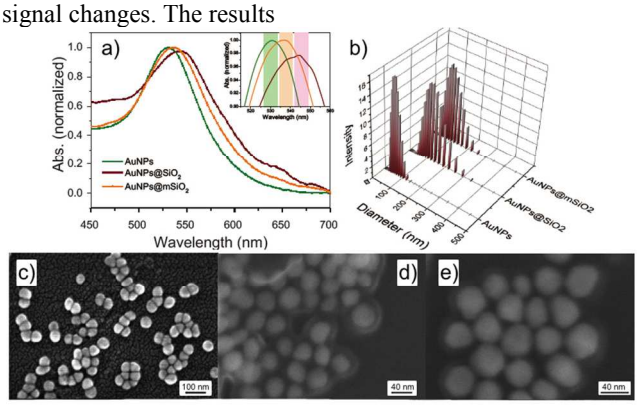

Figure 1. Characterization of AuNPs, AuNPs@SiO$_2$ and AuNPs@mSiO$_2$. a) Absorption spectra of AuNPs, AuNPs@SiO$_2$ and AuNPs@mSiO$_2$ (inset: the partial enlarged details of the absorption spectra). b) Dynamic light scattering data of AuNPs, AuNPs@SiO$_2$ and AuNPs@mSiO$_2$. c-e) SEM of AuNPs, AuNPs@SiO$_2$ and AuNPs@mSiO$_2$, respectively.

ensured that these two rhodamine spirolactam were specifically responded to the target metal ions.

Rhodamine spirolactam derivatives loading quantity on the AuNPs@mSiO$_2$. Rhodamine spirolactam derivatives had two absorption bands at 271 nm and 332 nm. Both of these absorption bands were used to calculate the loading quantities (Table 1). Rhodamine spirolactam and their derivatives could be adsorbed on the surface of AuNPs via electrostatic interaction. Therefore, we evaluated the loading quantities for both AuNPs and AuNPs@mSiO$_2$ (Figure S4). The spectra indicated that the addition of AuNPs could decrease the absorbance of RhB-HA and RhB-EDA in the supernatant, and 6.04 μM RhB-HA or 2.98 μM RhB-EDA could be loaded to AuNPs owning to this electrostatic adherence. However, AuNPs@mSiO$_2$ could load more rhodamine spirolactam than bare AuNPs according to the absorption spectra since the molecules could entered the gaps on AuNPs@mSiO$_2$. As we calculated, 7.88 μM for RhB-HA or 13.1 μM for RhB-EDA was loaded to the AuNPs@mSiO$_2$, averagely increased 30.46% and 339.6%. Therefore, the purpose to loading more molecules by using mesoporous silica was successfully achieved.

Target detecting via PRET process between RhB derivatives and AuNPs. The strong overlaps between the LSPR-LS of AuNPs and the absorption of rhodamine guaranteed a proper PRET process could be generated from them. By altering the rhodamine spirolactam derivatives embedded in the AuNPs@mSiO$_2$, different targets could be detected (RhB-HA for Cu^{2+} and RhB-EDA for Hg^{2+}, Figure 2a and 2d). In order to confirm the LSPR-LS signal was generated by single AuNPs@mSiO$_2$, colocation of nanoparticles by SEM and DFM was firstly evaluated. DFM image presented five green scattering light spots and collocating SEM image indicated they are five separated AuNPs. (Figure S5) Therefore, we deemed that the PRET process was occurred between single AuNPs@mSiO$_2$ and rhodamine spirolactam derivatives. To observe the PRET process, the LSPR-LS changes of RhB-HA doped AuNPs@mSiO$_2$ was firstly examined. The addition of Cu^{2+} could react with RhB-HA and arouse the ring-opening process of the RhB-HA, which restored the absorption around

550 nm and generated the PRET process. As figure 2b showed, the scattering signal was quenched gradually after the addition of Cu^{2+} in 10 minutes. To confirm the quenching effect, dynamic scattering light intensities variation of three different scattering

Table 1. Loading quantities of rhodamine spirolactam derivatives for both AuNPs and AuNPs@mSiO$_2$

	Examining wavelength	derivatives[a] Absorbance	load in AuNPs[b] Absorbance	Doping quantity (μM)	load in AuNPs@*m*SiO$_2$[b] Absorbance	Doping quantity (μM)
RhB-HA	271 nm	0.865	0.755	6.36	0.722	8.09
	310 nm	0.332	0.294	5.72	0.281	7.68
RhB-EDA	272 nm	0.714	0.695	1.33	0.536	12.5
	313 nm	0.281	0.255	4.63	0.204	13.7

[a] The concentration of rhodamine spirolactam derivatives was 50 μM.
[b] The concentration of AuNPs and AuNPs@*m*SiO$_2$ were 33.2 pM.

spots (1 to 3) were investigated by hue-saturation-intensity (HSI) color model as previous reports (Figure S6).[47] The intensities of these three spots dropped from 17457, 9588 and 8186 to 5011, 2290 and 1785 with average quenching efficiency of 0.7520 ± 0.0354. To further confirming the PRET process between RhB-HA and AuNPs, time-spectra 2-D profile of single AuNP was used to monitor the variations (Figure 2c). The spectrum of single AuNP at 0 min presented a peak at 553 nm with intensity of 9130.7, and the scattering light intensity deceased to 3387.6 gradually within 10 minutes. The quenching efficiency from spectra intensity was 0.6290. Meanwhile, the peak of scattering light spectra shifted 18 nm to 571 nm. This phenomenon was aroused by the absorption of RhB-HA as previous report.[23]

To further confirm the generality of this method, RhB-HA was changed to RhB-EDA. The spirolactam structure of RhB-EDA could be sabotaged by Hg^{2+}, generate the absorption around 550 nm and interact with AuNPs via PRET process. Same characterizations were performed. Dynamic scattering light images indicated that the addition of Hg^{2+} could significantly quenched the scattering light of AuNPs within 10 min (Figure 2e). The scattering light intensities of spots 4 to 6 were also measured by HSI color model. The intensities were 50213, 27422 and 14692 before the addition of mercury ions, which dropped to 15127, 7758 and 4187 after 10 minutes (Figure S6), with an efficiency of 0.6969 ± 0.0242. Time-spectra 2-D profile of individual AuNP was also performed to confirm the PRET process (Figure 2f). Analogous to the detection of Cu^{2+}, the addition of Hg^{2+} could quenched the spectrum of single AuNP from 9599.5 to 3017.3 with a quenching efficiency of 0.6857. The peak similarly shifted 15 nm from 560 nm to 571 nm due the absorption band of RhB-EDA. These two experiments indicated that by simply changing the rhodamine spirolactam derivatives, this PRET involved method could be applied to other target detection. Control experiments were also preformed to evaluate the necessity of silica coated AuNPs. As Figure S7 indicated, even though uncoated AuNPs could adsorb rhodamine spirolactam molecules on the surface, the quenching efficiency was less than that of the AuNPs@mSiO$_2$, especially for the circumstance of Hg^{2+} detection since the loading efficiency for RhB-EDA on AuNPs@mSiO$_2$ was far more than the efficiency of AuNPs. The selectivity of the detection was investigated. All the interfering ions could not significantly quench the scattering lights of AuNPs@mSiO$_2$ comparing to the addition of Cu^{2+} (Figure S8) or Hg^{2+} (Figure S9). This phenomenon resulted from the specific selectivity of RhB-EDA or RhB-HA.

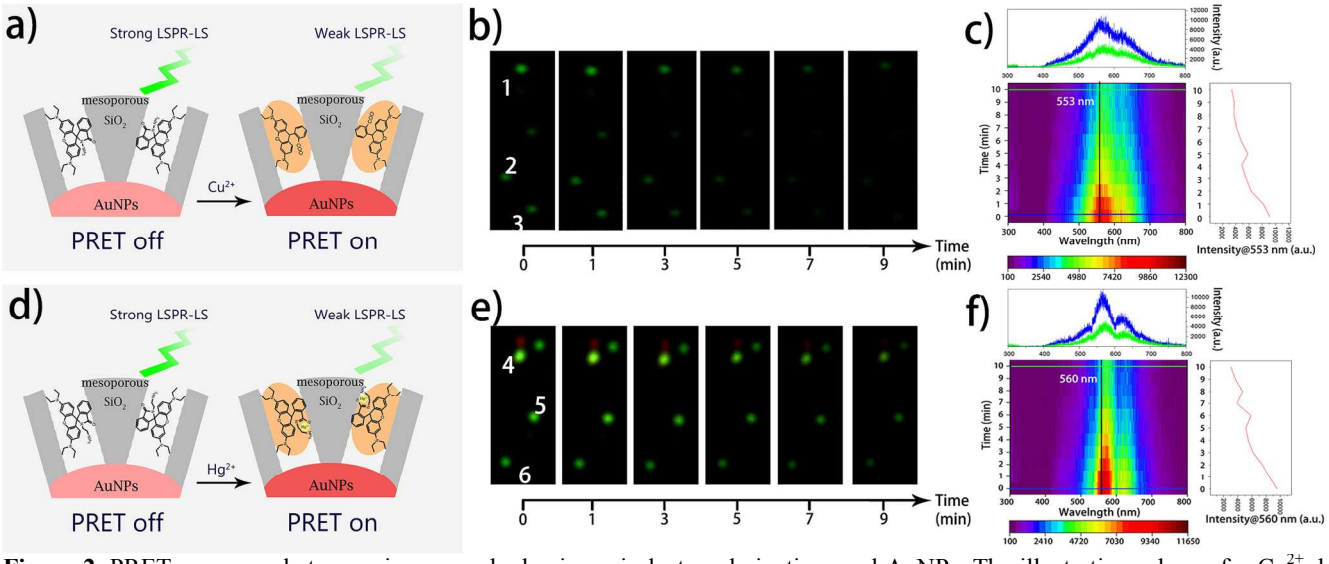

Figure 2. PRET processes between ring-open rhodamine spirolactam derivatives and AuNPs. The illustrating scheme for Cu^{2+} detection by RhB-HA (a) and the illustrating scheme for Hg^{2+} detection (d); The dark field images of RhB-HA doped AuNPs@mSiO$_2$ within 10 minutes after the Cu^{2+} addition (b) and the dark field images of RhB-EDA doped AuNPs@mSiO$_2$ within 10 minutes after the Hg^{2+} addition (e); The scattering light spectra profile of single RhB-HA doped AuNP@mSiO$_2$ after the Cu^{2+} addition (c) and the scattering light spectra profile of single RhB-HA doped AuNP@mSiO$_2$ after the Cu^{2+} addition (f). [Cu^{2+}] = [Hg^{2+}] = 100 μM.

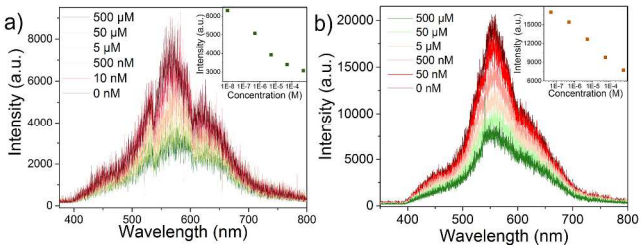

Figure 3. The scattering light spectra with different concentrations of targets. a) The scattering light spectra of single RhB-HA doped AuNP@mSiO$_2$ with different concentrations of Cu^{2+}, inset: the intensity distribution according to the spectra; b) The scattering light spectra of single RhB-EDA doped AuNP@mSiO$_2$ with different concentrations of Hg^{2+}, inset: the intensity distribution according to the spectra.

Different concentrations of Cu^{2+} and Hg^{2+} were applied to this PRET detecting system, and spectra of single AuNP were measured accordingly (Figure 3a). Within 10 nM Cu^{2+} ions, the scattering light spectrum intensity could be slightly quenched from 7025 to 6296. By increasing the concentration of Cu^{2+}, more severe quenching phenomenon could be observed. However, for the circumstance which Cu^{2+} was over 500 μM, the spectra could barely be quenched. Same quenching process could be observed in the Hg^{2+} detection (Figure 3b). With the addition of 50 nM Hg^{2+}, the spectra intensity dropped from 20219 to 17002. The intensity quenched gradually with the increase of Hg^{2+}. These phenomena proved that certain relationship was between the concentrations of target and scattering light intensities, and significant potential could be found in further applications. Compared to other PRET based Cu^{2+} detecting methods, detection limit of this method was comparable.[17, 21, 37] When same routine was applied for Hg^{2+} detection, high sensitivity could also be achieved. We believe the general method could be used for other metal ions detection with high sensitivity by simply change the rhodamine spirolactam molecules.

Theoretical simulation of the PRET between RhB derivatives and AuNPs@mSiO$_2$. We have proved the occurrence of PRET between AuNPs and tetramethyl-6-carboxyrhodamine (TAMRA) experimentally and theoretically in previous work [23]. For further understanding the interaction between RhB derivatives and AuNPs@mSiO$_2$, finite-difference time-domain (FDTD) simulation were used to investigate.[48-50] The composite shell was considered as a dielectric material and Maxwell-Garnett rule was applied.[51,52] The shell was constructed by RhB derivatives doped mesoporous silica, and the permittivity of RhB derivative was described as one simple harmonic oscillator by single Lorentzian function:[23,53]

$$\varepsilon_i = \varepsilon_{bg} - s\omega_0^2 / (\omega^2 - \omega_0^2 + i2\omega\gamma) \quad (1)$$

the real part and imaginary part of the complex dielectric function could be separated and wrote as:

$$\varepsilon_i^{Re} = \varepsilon_{bg} + [s\omega_0^2(\omega_0^2 - \omega^2)]/[(\omega_0^2 - \omega^2)^2 + 4\omega^2\gamma^2] \quad (2)$$

$$\varepsilon_i^{Im} = 2s\omega\omega_0^2\gamma/[(\omega_0^2 - \omega^2)^2 + 4\omega^2\gamma^2] \quad (3)$$

where ε_i was the complex dielectric function of the doping material (RhB derivatives), ε_{bg} represents the high-frequency component of the dielectric function. The frequency of the molecular transition of RhB derivatives is given by ω_0, s and γ are the oscillator strength and the line width of the RhB derivatives molecular transition, respectively. Considering both the ring-opened RhB-HA and the RhB-EDA were analogous to TAMRA, and the single Lorentzian function only evaluate the peak of absorption spectrum,[48,49] same s and γ values were applied to this simulation for simplification. Rayleigh mixing formula was used to combine the complex dielectric functions of these two components:[54]

$$\varepsilon_{eff} = \varepsilon_e + 3f\varepsilon_e \frac{\varepsilon_i - \varepsilon_e}{\varepsilon_i + 2\varepsilon_e - f(\varepsilon_i - \varepsilon_e)} \quad (4)$$

where ε_{eff} was the complex dielectric function of the composite material, ε_e was the complex dielectric function of the substrate (mesoporous silica), f was the fraction of the volume occupied by doping material. By continuous transforming f from 0 to 1, both the real part and imaginary part of the complex dielectric function increased (Figure 4a, 4b and S10). The increasing value of imaginary part manifested itself physically by absorption of more electromagnetic energy in the medium.[53] The complex dielectric functions were further applied in the FDTD simulations. The electric field was distributed around the AuNP core when only silica shell (f = 0) was coated on the surface. However, once the RhB derivatives were doped in the shell nanostructure, the electric field on the AuNPs was severely dwindled and the distribution moved to the surface of shell (Figure 4c and S11). The simulation suggested that the RhB derivatives increased value of complex permittivity of the composite shell nanostructure and aroused a stronger interaction with the electric field of AuNPs. This could be the primary cause of the scattering light quenching.

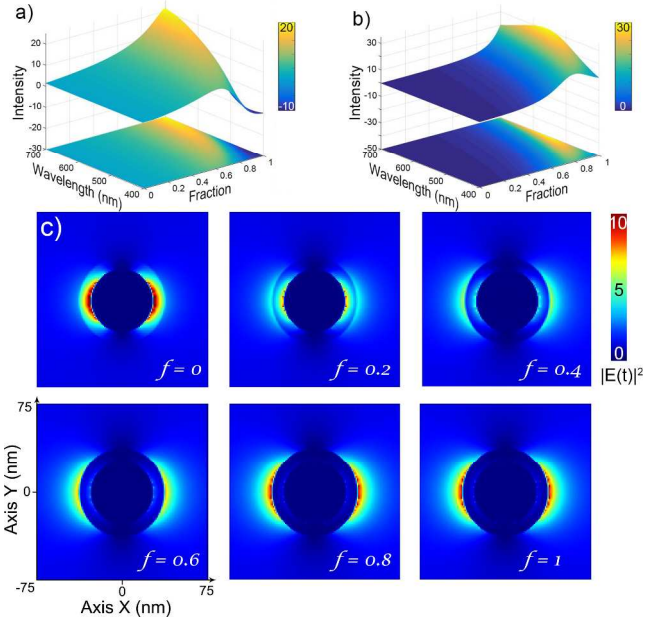

Figure 4. Theoretical simulations of the PRET between rhodamine spirolactam derivatives and AuNPs@mSiO$_2$. a-b) the real part (a) and the imaginary part (b) of the complex dielectric function of the composite shell determined by Rayleigh mixing formula on different fraction value. c) FDTD simulations for the electric field distribution of rhodamine doped AuNPs@mSiO$_2$ on different fraction value at XY plane.

CONCLUSIONS

A general method was established for target detection via PRET process between RhB derivatives and AuNPs. As a proof of concept, two different rhodamine spirolactam derivatives were synthesized as sensor to detecting Cu^{2+} and Hg^{2+} respectively due to the ring-open process. AuNPs@mSiO$_2$ was synthesized for better loading efficiency. The rhodamine spiro-

lactam derivatives doped AuNPs@mSiO$_2$ manifested highly specific reaction to the targets within 10 minutes. Theoretical simulations indicated the ring-opened rhodamine spirolactam derivatives could increase the value of the permittivity of the shell structure, result a strong interaction with the electric field of AuNPs, which caused the quench of the scattering light. This detecting method could provide an *in situ* observing and sensing platform for targets. By simply change the rhodamine spirolactam derivatives, this method could be used to detect other specific targets, such as anions, cations or small molecules, which provided a potential general method for sensing based on single nanoparticle.

ASSOCIATED CONTENT

Supporting Information

Supporting Information Available: ^{1}H NMR and ^{13}C NMR of RhB-HA and RhB-EDA, absorption spectra of loading quantity measurement, colocation image, HSI intensity, *i*DFM image for selectivity, variation of complex dielectric function and electric field intensity distribution. This material is available free of charge via the Internet at http://pubs.acs.org.

AUTHOR INFORMATION

Corresponding Author

* chengzhi@swu.edu.cn

Author Contributions

The manuscript was written through contributions of all authors. All authors have given approval to the final version of the manuscript.

Notes

The authors declare no competing financial interest.

ACKNOWLEDGMENT

This research was financially supported by the National Natural Science Foundation of China (NSFC, Grant No. 21535006).

REFERENCES

(1) Clapp, A. R.; Medintz, I. L.; Mauro, J. M.; Fisher, B. R.; Bawendi, M. G.; Mattoussi, H. *J. Am. Chem. Soc.* **2004**, *126*, 301-310.
(2) Freeman, R.; Liu, X.; Willner, I. *J. Am. Chem. Soc.* **2011**, *133*, 11597-11604.
(3) Lee, J. S.; Joung, H. A.; Kim, M. G.; Park, C. B. *ACS Nano* **2012**, *6*, 2978-2983.
(4) Li, M.; Wang, Q.; Shi, X.; Hornak, L. A.; Wu, N. *Anal. Chem.* **2011**, *83*, 7061-7065.
(5) Liu, G. L.; Long, Y. T.; Choi, Y.; Kang, T.; Lee, L. P. *Nat. Methods* **2007**, *4*, 1015-1017.
(6) Sapsford, K. E.; Berti, L.; Medintz, I. L. *Angew. Chem. Int. Ed.* **2006**, *45*, 4562-4589.
(7) Dong, Y. P.; Zhou, Y.; Wang, J.; Zhu, J. J. *Anal. Chem.* **2016**, *88*, 5469-5475.
(8) Zhang, J.; Cheng, F.; Li, J.; Zhu, J.-J.; Lu, Y. *Nano Today* **2016**, *11*, 309-329.
(9) Griffin, J.; Singh, A. K.; Senapati, D.; Rhodes, P.; Mitchell, K.; Robinson, B.; Yu, E.; Ray, P. C. *Chem. Eur. J.* **2009**, *15*, 342-351.
(10) Jennings, T. L.; Singh, M. P.; Strouse, G. F. *J. Am. Chem. Soc.* **2006**, *128*, 5462-5467.
(11) Giljohann, D. A.; Seferos, D. S.; Daniel, W. L.; Massich, M. D.; Patel, P. C.; Mirkin, C. A. *Angew. Chem. Int. Ed.* **2010**, *49*, 3280-3294.
(12) Marinakos, S. M.; Chen, S.; Chilkoti, A. *Anal. Chem.* **2007**, *79*, 5278 - 5283.
(13) Kalita, M.; Balivada, S.; Swarup, V. P.; Mencio, C.; Raman, K.; Desai, U. R.; Troyer, D.; Kuberan, B. *J. Am. Chem. Soc.* **2014**, *136*, 554-557.
(14) Yun, C. S.; Javier, A.; Jennings, T.; Fisher, M.; Hira, S.; Peterson, S.; Hopkins, B.; Reich, N. O.; Strouse, G. F. *J. Am. Chem. Soc.* **2005**, *127*, 3115-3119.
(15) Long, Y. T.; Jing, C. *Localized Surface Plasmon Resonance Based Nanobiosensors*; Springer: Berlin Heidelberg, 2014.
(16) Zhang, L.; Li, Y.; Li, D. W.; Jing, C.; Chen, X.; Lv, M.; Huang, Q.; Long, Y. T.; Willner, I. *Angew. Chem. Int. Ed.* **2011**, *50*, 6789-6792.
(17) Choi, Y.; Park, Y.; Kang, T.; Lee, L. P. *Nat. Nanotechnol.* **2009**, *4*, 742-746.
(18) Qu, W.-G.; Deng, B.; Zhong, S.-L.; Shi, H.-Y.; Wang, S.-S.; Xu, A.-W. *Chem. Commun.* **2011**, *47*, 1237-1239.
(19) Xu, X.; Chen, Y.; Wei, H.; Xia, B.; Liu, F.; Li, N. *Anal. Chem.* **2012**, *84*, 9721-9728.
(20) Li, T.; Xu, X.; Zhang, G.; Lin, R.; Chen, Y.; Li, C.; Liu, F.; Li, N. *Anal. Chem.* **2016**, *88*, 4188-4191.
(21) Jing, C.; Shi, L.; Liu, X.; Long, Y. T. *Analyst* **2014**, *139*, 6435-6439.
(22) Cao, Y.; Xie, T.; Qian, R. C.; Long, Y. T. *Small* **2016**.
(23) Gao, M. X.; Zou, H. Y.; Gao, P. F.; Liu, Y.; Li, N.; Li, Y. F.; Huang, C. Z. *Nanoscale* **2016**, *8*, 16236-16242.
(24) Medintz, I.; Hildebrandt, N. *FRET - Forster Resonance Energy Transfer_ From Theory to Applications*; Wiley-VCH Verlag GmbH & Co. KGaA: Germany, 2014.
(25) Schuller, J. A.; Barnard, E. S.; Cai, W.; Jun, Y. C.; White, J. S.; Brongersma, M. L. *Nat. Mater.* **2010**, *9*, 193-204.
(26) Gao, P. F.; Gao, M. X.; Zou, H. Y.; Li, R. S.; Zhou, J.; Ma, J.; Wang, Q.; Liu, F.; Li, N.; Li, Y. F.; Huang, C. Z. *Chem. Sci.* **2016**, *7*, 5477-5483.
(27) Jain, P. K.; Lee, K. S.; El-Sayed, I. H.; El-Sayed, M. A. *J Phys Chem B* **2006**, *110*, 7238-7248.
(28) Choi, Y.; Kang, T.; Lee, L. P. *Nano Lett.* **2009**, *9*, 85-90.
(29) Chatterjee, A.; Santra, M.; Won, N.; Kim, S.; Kim, J. K.; Kim, S. B.; Ahn, K. H. *J. Am. Chem. Soc.* **2009**, *131*, 2040-2041.
(30) Li, W.; Wang, W.; Yang, Y.; Zhang, K. *J. Mater. Chem. A* **2014**, *2*, 13675-13681.
(31) Reddy, G. U.; Ali, F.; Taye, N.; Chattopadhyay, S.; Das, A. *Chem. Commun.* **2015**, *51*, 3649-3652.
(32) Yuan, L.; Lin, W.; Zheng, K.; Zhu, S. *Acc. Chem. Res.* **2013**, *46*, 1462-1473.
(33) Zhu, H.; Fan, J.; Xu, Q.; Li, H.; Wang, J.; Gao, P.; Peng, X. *Chem. Commun.* **2012**, *48*, 11766-11768.
(34) Dujols, V.; Ford, F.; Czarnik, A. W. *J. Am. Chem. Soc.* **1997**, *119*, 7386-7387.
(35) Kaushansky, A.; Allen, J. E.; Gordus, A.; Stiffler, M. A.; Karp, E. S.; Chang, B. H.; MacBeath, G. *Nat. Protoc.* **2010**, *5*, 773-790.
(36) Sun, S.; Gao, M.; Lei, G.; Zou, H.; Ma, J.; Huang, C. *Nano Res.* **2016**, *9*, 1125-1134.

(37) Cao, Y.; Lin, Y.; Qian, R. C.; Ying, Y. L.; Si, W.; Sha, J.; Chen, Y.; Long, Y. T. *Chem. Commun.* **2016**, *52*, 5230-5233.
(38) Shi, L.; Jing, C.; Gu, Z.; Long, Y. T. *Sci. Rep.* **2015**, *5*, 10142.
(39) Harada, M. *Crit. Rev. Toxicol.* **2008**, *25*, 1-24.
(40) Nolan, E. M.; Lippard, S. J. *J. Am. Chem. Soc.* **2003**, *125*, 14270-14271.
(41) Gaggelli, E.; Kozlowski, H.; Valensin, D.; Valensin, G. *Chem. Rev.* **2006**, *106*, 1995-2044.
(42) Graf, C.; Vossen, D. L. J.; Imhof, A.; van Blaaderen, A. *Langmuir* **2003**, *19*, 6693-6700.
(43) Ge, J.; Zhang, Q.; Zhang, T.; Yin, Y. *Angew. Chem. Int. Ed.* **2008**, *47*, 8924-8928.
(44) Hasegawa, T.; Kondo, Y.; Koizumi, Y.; Sugiyama, T.; Takeda, A.; Ito, S.; Hamada, F. *Bioorg. Med. Chem.* **2009**, *17*, 6015-6019.
(45) Sasaki, H.; Hanaoka, K.; Urano, Y.; Terai, T.; Nagano, T. *Bioorg. Med. Chem.* **2011**, *19*, 1072-1078.
(46) Weerasinghe, A. J.; Schmiesing, C.; Sinn, E. *Tetrahedron Lett.* **2009**, *50*, 6407-6410.
(47) Liu, Y.; Huang, C. Z. *Chem. Commun.* **2013**, *49*, 8262-8264.
(48) Antosiewicz, T. J.; Apell, S. P.; Shegai, T. *ACS Photonics* **2014**, *1*, 454-463.
(49) Chen, H.; Shao, L.; Woo, K. C.; Wang, J.; Lin, H.-Q. *J. Phys. Chem. C* **2012**, *116*, 14088-14095.
(50) Juluri, B. K.; Lu, M.; Zheng, Y. B.; Huang, T. J.; Jensen, L. *J. Phys. Chem. C* **2009**, *113*, 18499-18503.
(51) Mallet, P.; Guérin, C. A.; Sentenac, A. *Phys. Rev. B* **2005**, *72*, 014205.
(52) Koledintseva, M. Y.; DuBroff, R. E.; Schwartz, R. W. *Prog. Electromagn. Res.* **2009**, *99*, 131-148.
(53) Bohren, C. F.; Huffman, D. R. *Absorption and Scattering of Light by Small Particles*; John Wiley & Sons, Inc., 1998.
(54) Sihvola, A. *Mixing Rules with Complex Dielectric Coefficients*; Kluwer Academic: Dordrecht, Netherlands, 2000; Vol. 1.

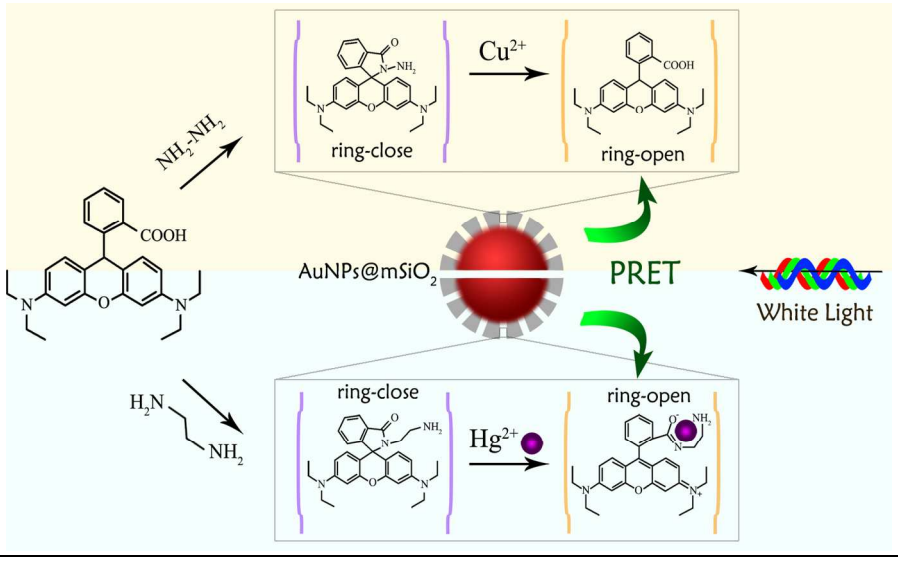
Cu2+
ring-close
ring-open
NH2-NH2
COOH
AuNPs@mSiO2
PRET
White Light
H2N
NH2
ring-close
ring-open
Hg2+